Modelling Heat Transfer of Timber Sections Subjected to Non-standard Fire Action

Abstract

Using timber as a structural material in buildings is promising in reducing the carbon footprint of construction, although fire safety has been a long-standing challenge prohibiting its wider use. The current design practice usually complies with Eurocode 5, but it is largely prescribed only for standard fire scenario. While investigating the fire behavior in real compartments containing timber members, the fire action imposed on the surface of timber members can be hardly represented by the standard fire curve. Therefore, modelling the heat transfer of timber sections in these real fire scenarios requires adequate numerical models. In this paper, the heat transfer model equipped with temperature-variant thermal properties of timber as well as a heat generation model addressing timber combustion effect, has been developed and implemented in the open-source simulation platform OpenSees for fire. Advancing from the existing heat transfer models, the present model has been validated against test results of timber sections subjected to the prescribed non-standard fire actions supported by the e-controlled radiant panel system. The modelling results have shown good performance in predicting the temperature evolution at various depths of the timber sections subjected to non-standard heating conditions.

Keywords: Fire exposure; heat transfer analysis; timber structure; thermal response; OpenSees

1. Introduction

Timber is widely used in building construction as non-structural and structural components. As a renewable construction material, it is a promising structural material to reduce the carbon footprint of modern urbanization while a decarbonized economy is pursued for the concern of climate change. To use timber as load-bearing components in structures, its performance at ambient conditions has been extensively investigated, such as tests on solid timber members subjected to combined axial force and bending moment [1], laminated lumber (LVL) members [2] and cross-laminated timber (CLT) panels under bending [3] and scrimber composite members subjected to axial compression [4]. However, the combustible nature of timber has been a long-existing barrier to the broader application in the construction industry, especially for multi-story buildings. Unlike conventional structural materials (i.e., concrete, steel, and masonry), unprotected timber sections can burn in a fire, and the resultant char layer can propagate from the surface to deeper layers within the section. Moreover, modern mass timber structures tend to leave the timber sections uncovered by fire protection layers. Therefore,

estimating the thermal response of such mass timber sections exposed to fires is a critical step in the fire safety design of timber structures. The current modelling practice provided in Eurocode 5 (EC5) [5] is only allowed to predict the thermal responses of timber sections in standard fire exposure [6, 7], which may be suitable in a prescriptive manner but not applicable to realistic fire scenarios with cooling phase [8] in building compartments especially for fires in large open-plan compartments [9-11]. For the latter fire scenarios, the fire exposure for timber sections experiences a cooling phase (decay period), during which the heat generated from burning timber plays an important role.

When timber sections are exposed to fire, a series of physical changes and chemical reactions occur. The initial wood layer is dehydrated as the moisture evaporates at around 100 °C. After dehydration, the wood is subjected to pyrolysis, which routinely occurs as slow pyrolysis below 200 °C, steady pyrolysis up to 300 °C and rapid pyrolysis above 300 °C [12, 13]. The combustible gases are the products of pyrolysis, after which the wood layer turns to a char layer (index temperature of charring is usually given as 300 °C) [14, 15]. The varying thermal properties of timber and its phase changes during fire exposure significantly complicate the heat transfer analysis, as both factors are temperature-dependent [13, 16, 17]. Experimental studies on the thermal response of timber sections have been conducted primarily using furnace fire tests prescribed in standard fire curve or parametric fire curve or using fixed heat fluxes in a cone calorimeter. A series of timber panel (1000 or 325 mm× 225 mm× 95 mm) tests were carried out by König and Walleij [18] to investigate one-dimensional charring of timber sections subjected to Standard fire (SF) and Parametric fire (PF). In these tests, the thermocouples at various thicknesses recorded the temperature variations and provided useful data for validating heat transfer models. White and Tran [19] used the cone calorimeter with various fixed heat fluxes (HF tests) ranging from 15 to 50 kW/m^2 to test the charring rate of different types of timber: pine, redwood, oak, and basswood. The reported work measured the timber temperature evolution at various depths, which offers rigorous reference to the modelling of timber response to a moderate range of heat fluxes. Tests on six kinds of Chinese softwood and hardwood were conducted by Wen et al. [20] using three different fixed heat fluxes (35, 50, 75 kW/m^2). Alongside the temperature data, the char depth growth in each test has been estimated using the thermocouple measured data with respect to the 300 °C isotherm. The average char rate in standard fire tests was around 0.65 mm/min as recommended in EC5 [5]. In the parametric fire tests [18] involving non-standard heating and a decay phase, the EC5 recommended values become not suitable to estimate the charring rate of timber sections subjected to these fire scenarios.

In EC5, the thermal properties of timber (i.e., density, conductivity, and specific heat) are given as temperature-dependent models, which formulates a model to address heat conduction only in timber sections, without consideration of heat generation from timber burning. To adapt the EC5 model to

non-standard fire scenarios, Zhang et al. [21] proposed an energy-based time-equivalent approach (EBTEA) to define equivalent standard fire load from non-standard fire exposure. This method provided a compromising approach for parametric fire scenarios while the heat of timber combustion remained ignored. Furthermore, heat release from timber combustion has not been considered in heat transfer models of timber sections [22]. Recent full-scale compartment tests by Bøe et al. [10] on open-plan CLT rooms showed that char oxidation on the exposed ceiling sustained during the cooling phase, which could trigger re-ignition. On the modelling side, Schmid and Frangi [23] proposed the Timber Charring and Heat Storage (TiCHS) model to quantify heat contribution from timber during post-flashover fire stages. Their framework incorporates the energy stored in the char layer and its gradual release during cooling. It is worth noting that the Gpyro model [24], which incorporates detailed micro-scale sub-models to represent complex chemical reactions (such as pyrolysis, charring, and oxidation) and associated physical changes (e.g., mass loss, phase transitions, and internal gas transport), has demonstrated high accuracy in simulating the thermal response of timber sections exposed to fire. Due to the technical complexity of a Gpyro model, an engineering model for timber structural design against various non-standard fire scenarios remains absent. The model proposed by Hopkin adopting a 'heat of hydration' principle described an easy-to-use model to account for the heat of timber combustion [25] was one attempt, which provides an inspiring methodology of considering the combustion heat but the model requires more consideration in heat release and validation against more non-standard fire scenarios. In addition, Floyd and Hodges [26] proposed a flux- and thickness-scaling method that converts cone-calorimeter data into an effective 'reference heat flux' for engineering-level pyrolysis prediction of wood, offering a practical, calibration-light alternative.

In this paper, modelling heat transfer of timber sections subjected to non-standard fire scenarios is explored and implemented in an open-source finite element modelling framework, which aims to provide an engineering-purposed and simplified model to account for heat transfer under fire action covering a wide range of heat fluxes in realistic fire scenarios (Fig. 1). A combustion heat estimation model based on laboratory test results has been proposed to approximate the heat absorbed by the timber section. The proposed model has been implemented in OpenSees [27] heat transfer module. The model is then validated against both test data reported in existing literature [18] and new experiments conducted in this study. In addition to the previous timber charring tests using parametric fire curves, the test data from the newly conducted tests using radiant panel system described in Section 3 is obtained for further validating the heat transfer models. The validation results have shown the overall good performance of the proposed model in estimating the thermal response of timber sections, demonstrating great potential in the implementation for fire safety design. As a part of open-source development, the source code and examples of this model have been made available at

openseesforfire.github.io, which allows continuous improvement of the model in future applications.

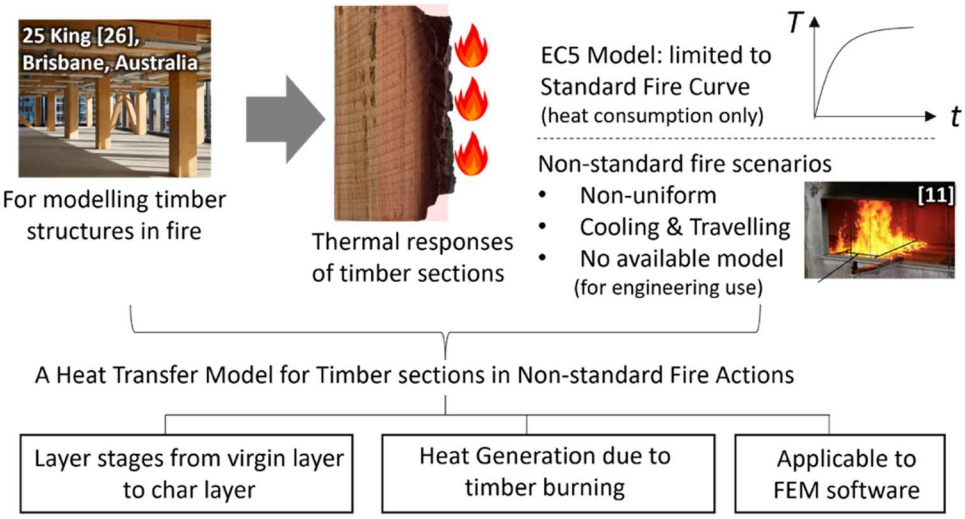

Fig. 1. The modelling needs for heat transfer model of timber sections exposed to non-standard fire [11, 28].

2. Background

2.1. Thermal Response and Layered States of Timber Exposed to fire

Timber surfaces exposed to fire are subject to the effect of external heat fluxes, resulting in the generation of flammable gas generation as pyrolysis products [12, 13]. As mentioned before, modelling the heat transfer of timber sections in fire should address the heat absorption as well as the heat generation [14, 15]. A timber layer routinely experiences different states namely virgin wood layer (virgin zone with the original moisture content), dried layer (dehydration zone), pyrolysis layer, char layer, and ash layer, as shown in Fig. 2a.

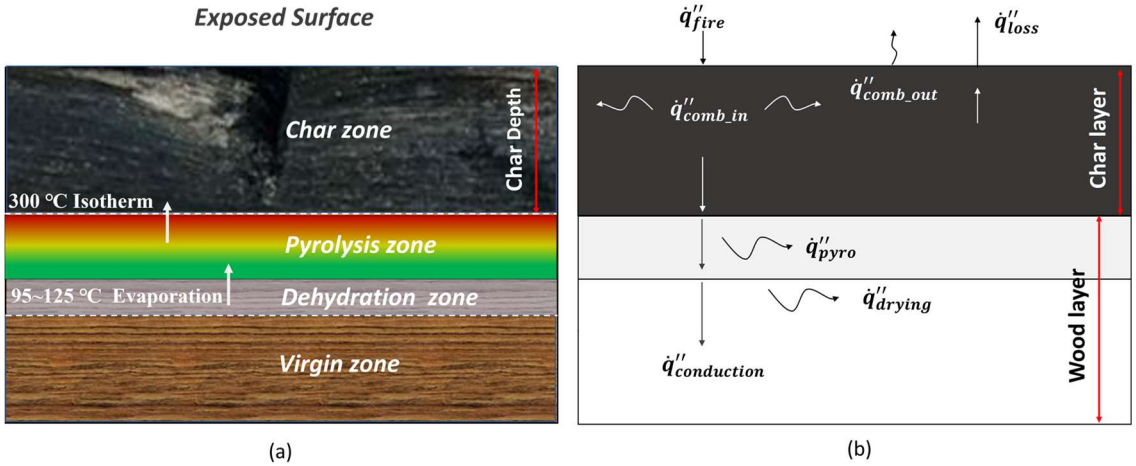

Fig. 2. Thermal response of timber exposed to fire: (a) Diagram of timber pyrolysis; (b) Heat transfer of timber section in fire.

When heated by an external fire, it is known that flames can sustain at the exposed surface of a timber section alongside the smouldering occurring in the charred layer underneath the flaming front.

In case where the external heating is not intense enough to sustain the surface flaming, smouldering becomes the dominant mode of oxidative combustion and leads to further pyrolysis. Flaming and smouldering are both exothermic oxidation reactions emitting heat to the room environment, and the absorbed portion by timber itself can significantly affect the thermal responses of timber sections. As illustrated in Fig. 2b, the gross heat of timber combustion is mostly released to the surrounding environment ($\dot{q}''_{comb\_out}$) in the form of flaming at the exposed surface of the timber and smouldering of the char layer. $\dot{q}''_{comb\_out}$ is not absorbed by the timber section, whereas the absorbed portion ($\dot{q}''_{comb\_in}$) contributes the heating to sustain the propagation of pyrolysis and charring. To quantify $\dot{q}''_{comb\_in}$, Section 3 introduces a comparative test using two heat flux gauges to measure the heat flux received from radiant panel and the heat flux received from both radiant panel and timber burning. The overall heat balance between the exposed surface and a deeper section of original wood may be expressed as:

$$\dot{q}''_{fire} - \dot{q}''_{loss} + \dot{q}''_{comb\_in} = \dot{q}''_{pyro} + \dot{q}''_{conduction} + \dot{q}''_{drying} \quad (1)$$

Where $\dot{q}''_{fire}$ represents the external heat flux at the exposed surface induced by room fire, and $\dot{q}''_{loss}$ is the heat loss at the exposed surface. The net input heat fluxes on the left-hand side of Eq. 1 are to balance the endothermic heat consumption processes ($\dot{q}''_{drying}$, $\dot{q}''_{pyrolysis}$) and the heat conduction to the deeper section $\dot{q}''_{conduction}$. When the timber section is tested using furnaces of prescribed time-temperature curves, such as standard fire, this additional heating impact owing to timber combustion becomes negligible because the $\dot{q}''_{fire}$ is dominated by the designated furnace temperature. However, if considering the actual fire development in a modern compartment, the additional heat contributed by the burning timber (primarily $\dot{q}''_{comb\_out}$) could cause the significant rise of $\dot{q}''_{fire}$ and change the fire behavior [9-11, 23]. Moreover, when the fire experiences a less intense period, the internally absorbed term, $\dot{q}''_{comb\_in}$, becomes the major heat resource to sustain the ongoing propagation of pyrolysis and charring. If the external heat flux further reduces, self-extinguishment of timber can occur. Apparently, an EC5 type model is not able to address such heat balance as no heat generation ($\dot{q}''_{comb\_in}$) is available. Therefore, in order to predict the thermal response of timber sections under non-standard fire actions, it is meaningful to establish a heat transfer model based on characteristic layer division and consider timber burning effects.

2.2. Existing Models and The Need for An Engineering Model for Non-standard Fires

Several models complement EC5 when fires are non-standard or include a decay phase as follows, however, these models either need limited fire scenarios (EC5 type model), detailed kinetics (Gpyro model), target compartment energy balances (TiCHS model), simplified sources (Hopkin model), or

limited testing scenarios and compartment boundary conditions consideration (Floyd & Hodges model). None directly deliver an engineering-oriented tool that both tracks layer states and incorporates heat generation from timber combustion under realistic fires with non-standard fire action.

Table 1. Existing heat transfer models for timber exposed to fires.

Model	Positioning	Applicability	Limits
EC 5 type (K&W [18] and M&B [16, 17, 29])	Semi-empirical, calibrated to SF/PF furnace tests	Reliable for 1D section response under SF/PF	Without heat generation from timber burning
TiCHS [21]	Energy-based time-equivalent approach	Captures decay-phase heating	Without heat generation from timber burning
Gpyro [24]	Mechanistic pyrolysis chemistry with coupled mass/energy transport	High accuracy for local phenomena and oxidation	Heavy data calibration and high computational cost
Hopkin [25]	Heat of hydration principle	Simple and fast	Requires calibration and broader validation for diverse non-standard fires
Floyd & Hodges [26]	Scaling-based engineering models	Multi-scale and multi-material	Limited testing scenarios (not modern large-open compartments); Real-compartment boundary conditions not fully covered

3. Newly Conducted Experimental Tests

To simplify and visualize the consideration of absorbed heat ($\dot{q}''_{comb\_in}$) when the char layer undergoes smouldering and being engulfed by surface flames, it is necessary to introduce a new method. The method was derived from a series of tests with the help of the Heat-Transfer Rate Inducing System (H-TRIS) [30], which was originally developed at University of Edinburgh. The H-TRIS established at Hong Kong Polytechnic University was employed in the present study, which is equipped with radiant panel matrix and electronically controlled moving rails. It allows for the time-varying heat fluxes on the exposed surface, which can be used to approximate various non-standard fire actions, as shown in Fig. 5a.

3.1. H-TRIS Series Tests for Deriving Heat Generation Model

3.1.1. Pre-test Procedure for Incident Heat Flux Uniformity Verification (Q_{fire1} vs Q_{fire2})

Two water-cooled heat flux gauges were calibrated under different heat flux conditions to measure incident radiative heat flux on the sample surface, $\boldsymbol{Q_{fire1}}$ and $\boldsymbol{Q_{fire2}}$, respectively. For all verifications, the sensing faces were oriented parallel to the radiant panel. To avoid the influence of accumulated

thermal gas around the heat flux gauges, based on the experience of Maluk et al. [31], the distance between the exposed surface of the rock wool board and the surface of the heat flux gauge inserted at its internal opening was set to 2 mm for calibration work. The corresponding experimental setup and layout are shown in Fig. 3. The calibration coefficients supplied by both gauge manufacturers were recorded for post-processing prior to use. The comparison in Fig. 3d confirms that, based on these calibration coefficients, the two gauges accurately measure the same incident radiant heat fluxes (within ± 2 %) within the entire 0-125 kW/m^2 calibration range

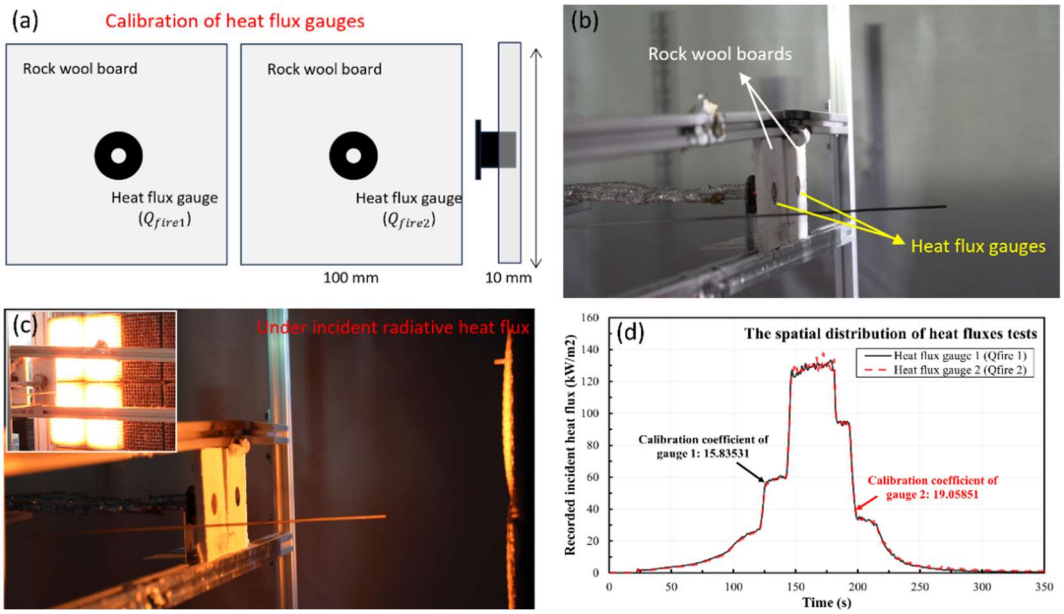

Fig. 3. Calibration procedure for heat flux gauges: (a) Schematic diagram of the pre-test device; (b) Experimental setup diagram; (c) Calibration under incident radiative heat flux applied by radiant panel; (d) The uniformity verification tests results for the two heat flux gauges used.

3.1.2. Incident vs Received Heat Flux Definitions (Q_{fire} vs Q_{total})

To quantify the heat transferred internally during the combustion process of timber, the tests were conducted by keeping the left side of the apparatus constant and replacing the right side with a timber block. A heat flux gauge was inserted into a pre-made hole to measure the heat flux, as shown in Fig. 4a and 4b. Subsequently, a series of tests were conducted to study the burning effects of timber under different fixed heat flux conditions for both components simultaneously. In this case, the reading of the heat flux gauge on the left side (rock wool board) is recorded as $\boldsymbol{Q_{fire}}$, which represents the incident radiant heat flux received at different distances. The reading of the heat flux gauge on the right side (timber block) is recorded as $\boldsymbol{Q_{total}}$, representing the heat effectively absorbed by the timber for the same incident radiant flux by considering the effects of timber combustion. Considering the gauge measured heat fluxes largely represent the flux components perpendicular to its surface, this may underestimate the heating contribution from timber burning and especially the oxidation of char layer.

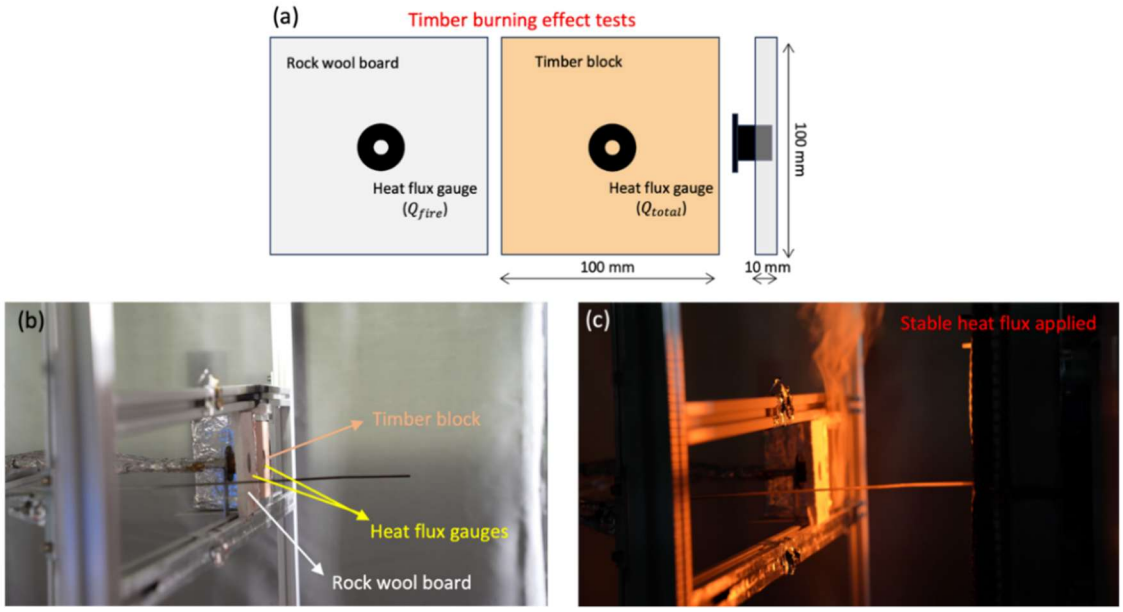

Fig. 4. Tests for quantifying the burning effects of timber: (a) Schematic diagram of the test device; (b) Experimental setup diagram; (c) Stable incident radiative heat flux applied by H-TRIS.

3.2. Newly Conducted Tests on Timber Sections Exposed to Non-standard fires for Validation

To investigate the effect of heat generation during timber combustion and to provide a more challenging case for validating the developed model, the newly conducted test under non-standard fire (NSF) actions characterized by varying heat flux has been conducted on European beech specimens with dimensions of 100 mm× 90 mm× 80 mm (Length × Width × Thickness) and modelled by using OpenSees for fire in this paper. The blocks were mounted 150 mm in front of the H-TRIS radiant panel, which delivered time-varying incident heat fluxes in the 0 - 125 kW/m^2 range under fully automatic power and rail control. Each specimen was oriented so that its 100 mm × 90 mm face was parallel to the panel. The remaining five faces were wrapped with 10-mm-thick aluminosilicate ceramic fibre and aluminum foil to maintain approximately one-dimensional (1D) heat transfer, as shown in Fig. 5b.

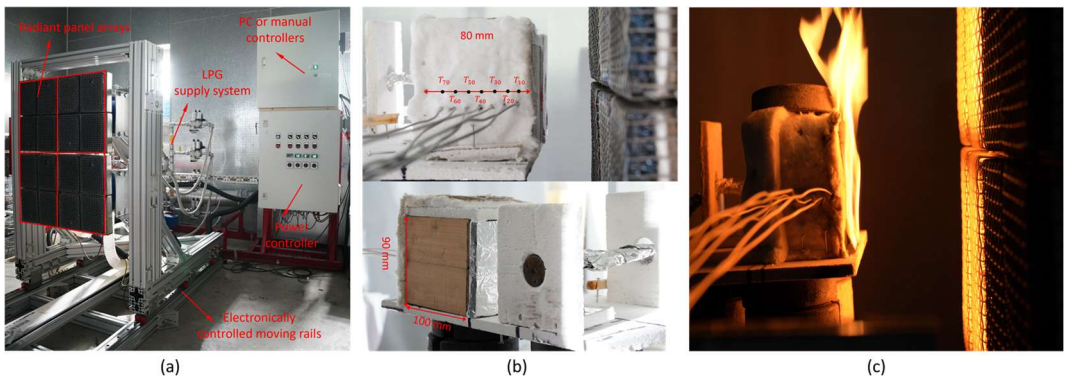

Fig. 5. A newly conducted non-standard fire test using H-TRIS radiant panels: (a) H-TRIS panels at Hong Kong PolyU; (b) A typical specimen with side insulation and thermocouples layout; (c) Flames at the timber surface during heating exposure.

Prescribed heat fluxes, varying over time in the 0 -125 kW/m^2 range, were applied to the timber blocks using the H-TRIS system's automatic rail and power control system. Type K thermocouples consisting of a 1.0 mm diameter thermocouple bead and stainless steel covered wire are placed in the timber section as shown in Fig. 5b, were installed 10, 20, 30, 40, 50, 60 and 70 mm from the exposed surface in timber section to record the temperature evolution. All sensing tips were embedded to depth of 50 mm by drilling 1.8 mm-diameter holes, inserting the junctions to depth, and backfilling the holes with ceramic paste to insulate. The sheathed leads were routed through an external layer of rock-wool insulation on the side surface. Therefore, the heat conduction from the heated thermocouple wires to the timber section should be minor. The average density of tested specimens in an ambient environment is 730 kg/m^3. The moisture ratio is 10.88% (samples with a sample variance of 6.31×10^{-5}), which is measured using specimens from the same batch regarding the initial weight G_0 at the ambient environment and the dry weight G_d after 24 hours of oven drying.

4. Development of Heat Transfer Model

4.1. Governing Equations and Boundary Conditions

The modelling of heat transfer in timber sections can be achieved in finite element software. The governing equation of it at element level is usually written in the following form [32]:

$$K_e \mathrm{T} + C_e \dot{\mathrm{T}} = Q_e \tag{2}$$

where K_e represents the conductive matrix of a finite element, and C_e is the thermal capacity matrix comprising specific heat c_p and density ρ. T is a vector of nodal temperature, $\dot{\mathrm{T}}$ indicates the temperature increment vector at the nodes, and Q_e represents the heat received at the element surfaces or internally generated, which can be estimated using the following equation:

$$Q_e = \int_S q_S \cdot \mathrm{d_S} + \int_V q_V \cdot \mathrm{d_V} \tag{3}$$

where q_S is the external heat flux vector received by the element if surface (S) heat fluxes exist. The volume heat q_V represents the internal volume (V) heat to separately consider the generated heat during the char oxidation of the timber section in this paper, which contrasts with the heat consumption of temperature rise corresponding to the heat capacity $C_e \dot{\mathrm{T}}$.

Furthermore, due to the complexity of physical changes and chemical reactions during the combustion process of timber, it is difficult to estimate the heat generated by timber combustion itself. As discussed previously, the heat generated by timber combustion ($\dot{q}''_{comb\_out}$) in the form of flaming and smouldering is largely released to the surrounding environment. Based on engineering simplification, this study relates the heat generated by the charring process and the received heat on

the surface through the heat generation model. This allows for an accurate and quick assessment of the impact of timber combustion. Therefore, when considering the effect of timber combustion, formula 3 can be rewritten as:

$$Q_e = \int_S q_S \cdot \mathrm{d_S} + \int_S kq_S \cdot \mathrm{d_S} \tag{4}$$

where k is the coefficient of variation which varies with the external incident heat flux and the corresponding variation follows the rules of the proposed heat generation model.

4.2. Implementation in OpenSees (phase-tag logic & cooling treatment)

As a leading open-source simulation framework, OpenSees [27] has been extended for modelling structures in fire [33]. In addition to the thermo-mechanical codes developed for structure responses, a transfer analysis module associated with a fire module has been added to the OpenSees for fire [33]. The HT analysis module has been equipped with Tcl and Python and validated previously [34]. In this paper, the above-discussed heat transfer model for timber is now implemented into the OpenSees heat transfer module and can be employed to model the temperature evolution in mass timber sections or timber-steel composite sections exposed to fire as shown in Fig. 6a.

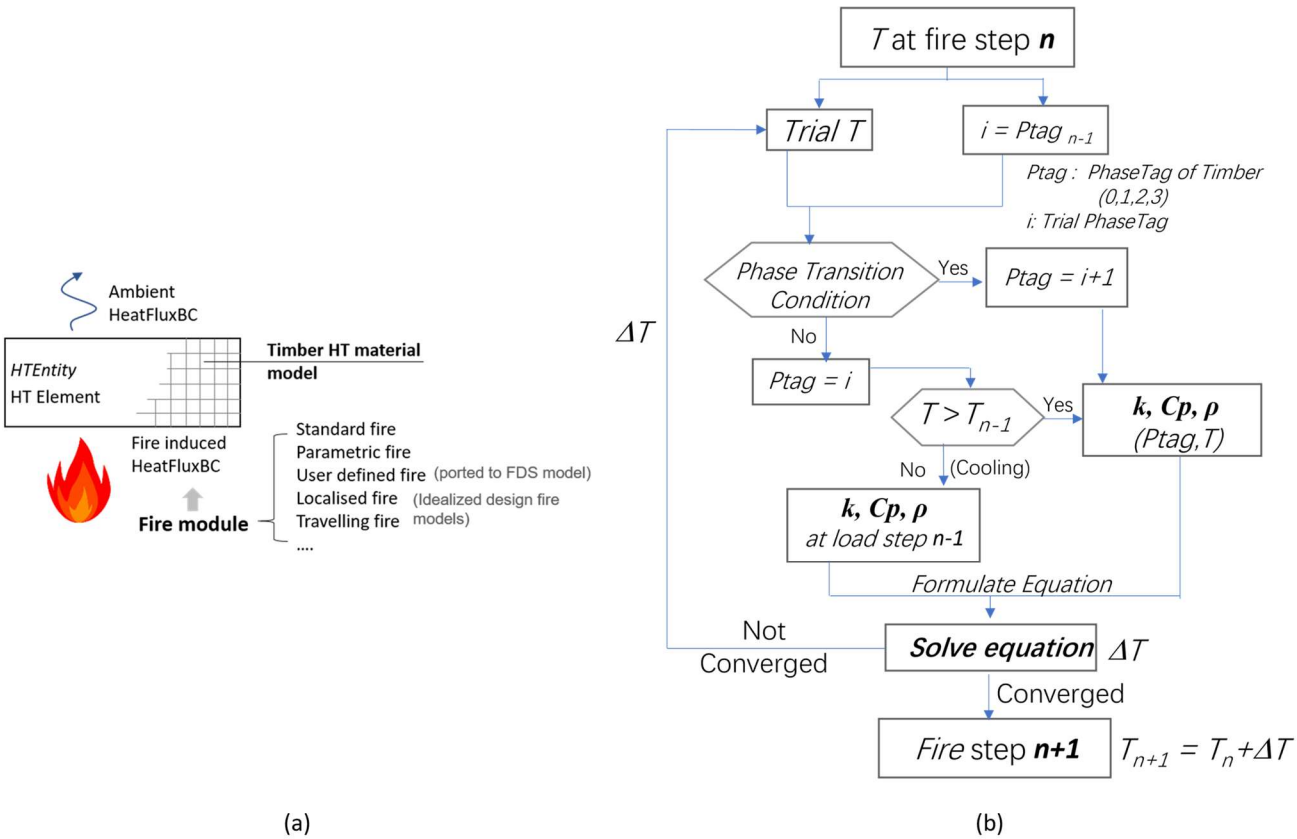

Fig. 6. Implementation of timber heat transfer material model based on finite element method: (a) Schematic of a heat transfer model; (b) State determination in FEM framework.

In Fig. 6b, a state determination process is given for the heat transfer model. At each Gaussian

Integration point of the finite element, a Phase Tag (Ptag) is assigned to the material model to record the current layer state corresponding to the various layers of timber section: the virgin layer (0), the dehydration layer (1), the pyrolysis layer (2), and the char layer (3). At each fire step $\boldsymbol{n}$, the trial temperature of the timber material will be updated with the trial ΔT after each iteration and the trial phase tag remains the committed tag. This will be checked against the phase transition conditions (critical temperature as mentioned earlier) to update the layer state, which is to prevent the reversed layer states associated with thermal properties during the cooling phase, e.g., a charred layer returning to 200ºC. In the cases of unchanged phase tag, the timber temperature will be compared to identify whether it enters a cooling stage. If yes, the timber layer will remain as the previously recorded state and its thermal properties will be taken as the committed values. Thus, during cooling, the char-tagged layer consistently maintains the thermal properties corresponding to the previously attained peak temperature, ensuring accurate and physically realistic heat transfer behavior throughout the timber section. If heating continues, the timber properties will be determined according to the updated phase tag and the trial temperature. These parameters will be set as committed values while the eventual convergence is fulfilled for the current load step.

4.3. Minimum-Input Layered Thermal Property Model

4.3.1. Minimum-Input Parameterization

To minimize the input of timber properties, the transitions of each thermal property are prescribed using linear curves, or the EC5 recommended variation when a specific input is not present. The model therefore requires only three baseline inputs at room temperature (20 °C by default): k_{20} for thermal conductivity, c_{p20} for specific heat, and ρ_{20} for density. Linearization is imposed for the implementation of temperature-based variation in OpenSees for fire, and all variations at elevated temperatures are controlled by these input parameters together with the prescribed transition curves (see Fig. 7, Table A.1-C_p, Table A.1-ρ and Table A.1-k in the Appendix). Unlike traditional approaches that rely solely on temperature, the proposed scheme assigns properties by a dual criterion, current temperature and the layer state, so that the section response remains well-posed during heating and cooling in realistic fires. The following subsection details the layered property laws and tag-based transitions

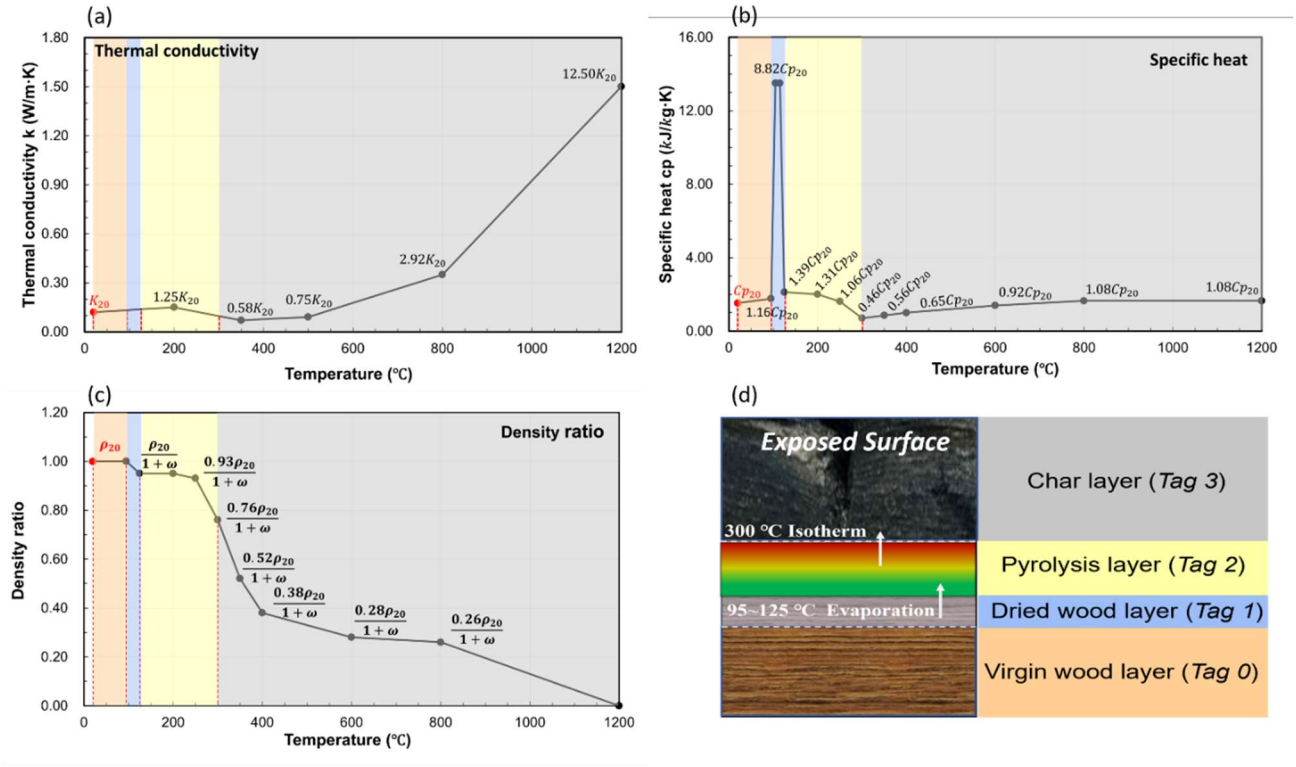

Fig. 7. Minimum-input parameterization of timber thermal properties and layered-state definition: (a) Thermal conductivity k; (b) Specific heat c_p; (c) Density ratio ρ/ρ_{20}; (d) Schematic of layer tags and temperature thresholds for timber section exposed to fires.

4.3.2. Layered-state Property Laws and Transitions

For thermal conductivity, the k_{20} was used as the control input parameter and adopt multi-segment bilinear curves that follow the EC 5 conductivity variation from 20 °C to 1200 °C. For specific heat, the input parameter c_{p20} is offered to allow flexible definition while generally following the EC 5 trend. For the purpose of finite element convergence, only the temperature range during the water evaporation stage was modified from the 99 °C – 99 °C (peak) – 120 °C (peak) - 120 °C to 95 °C – 105 °C (peak) – 115 °C (peak) - 125°C [35, 36]. In detail, the specific heat increases linearly from $\boldsymbol{c_{p20}}$ to $1.16\boldsymbol{c_{p20}}$ at 20 °C to 95°C, which is followed by a linear surge to $8.86\boldsymbol{c_{p20}}$ representing the massive heat consumption due to evaporation (105 °C - 115 °C). A liner declines from $8.86\boldsymbol{c_{p20}}$ to $1.39\boldsymbol{c_{p20}}$ at 125 °C indicates the completed drying process. The density variation adopts an identical model as recommended in EC5, which depends on the original wood density $\boldsymbol{\rho_{20}}$ and moisture ratio w. Except for the specific-heat adjustment around evaporation, the thermal properties of timber (k, c_p, and ρ) are thus taken from existing layered property models [16-18, 29] and EC5 and consistently parameterized by (k_{20}, c_{p20}, and ρ_{20}) without case-by-case calibration.

Based on the transition conditions between different stages of timber pyrolysis, layer tags are used in the proposed heat transfer model to record the distribution of characteristic layers within the timber

cross-section during a fire. The thermal properties of each characteristic layer would be based on its temperature and layer tag. For the transition conditions, the change from the virgin layer (*Tag 0*) to the dehydration layer (*Tag 1*) is determined by the evaporation temperature of 95 °C and the dehydration process is completed in the range of 95 °C to 125 °C. Upon completion of dehydration, the dehydration layer (*Tag 1*) transforms into the pyrolysis layer (*Tag 2*), which starts the initial slow pyrolysis. The critical temperature for determining the transition to the char layer (*Tag 3*) is assigned as 300 °C, as it is usually recommended in the literature for identifying the char front. Once the transition between layers is achieved, no backward transition should be allowed, and the layer state tag will remain as the higher one, e.g., the formed char layer cannot be regressed to a wood layer. Consequently, the thermal properties of each layer are based on its temperature and tag, and during cooling the variables are determined by the past maximum temperature ("peak-temperature locking") in each layer state. This ensures that the char formed during the heating stage (*Tag 3*) retains the appropriate properties during subsequent cooling, preventing unphysical rollback and enabling accurate, quick assessment of heat transfer under non-standard fires with cooling.

For application, the key input parameters are defined according to consistent principles, (k_{20}, c_{p20}, and ρ_{20}) for the base material and w when density-moisture coupling is needed, while any missing temperature dependence defaults to EC5. Case execution then simply selects the material baselines and boundary conditions, after which the prescribed curves and layer tags govern the full-range property transitions (20 – 1200 °C) without specific calibration for each modelling case.

4.4. Heat Generation Model to Consider Timber Burning Effect

Timber, as a typical charring material, can sustain both flaming and smoldering combustion and once ignited, timber elements in compartments contribute significantly to the overall heat release rate and potentially affect the fire resistance of the overall structure. The tests mentioned in Section 3.1 above explored the values of the external incident heat flux ($\boldsymbol{Q_{fire}}$) and the received total heat flux ($\boldsymbol{Q_{total}}$), which aims to establish a protocol of a simple heat generation model to be integrated in the heat transfer model of timber sections subjected to non-standard fires, as shown in Fig. 8a. Specifically, the maximum $\boldsymbol{Q_{fire}}$ in the heat-generation model was limited to 125 kW/m^2, corresponding to the highest measured surface heat flux of the present H-TRIS setup. Furthermore, based on the characteristics of the test data distribution, the overall fitting of the relationship curves when $\boldsymbol{Q_{fire}}$ changes within the 0~125 kW/m^2 heating stage and 125~0 kW/m^2 cooling stage, and the formula of the trend fitting curve is shown in Equation (5), respectively,

$$Q_{total} = \begin{cases} 3.40e^{-5}\left(Q_{fire}\right)^3 - 3.75e^{-3}\left(Q_{fire}\right)^2 + 1.27Q_{fire}, & 0 < Q_{fire} < 125 \\ 6.67e^{-8}\left(Q_{fire}\right)^5 + 2.15e^{-5}\left(Q_{fire}\right)^4 - 2.44e^{-3}\left(Q_{fire}\right)^3 + 0.11\left(Q_{fire}\right)^2 + 0.42Q_{fire}, & 125 > Q_{fire} > 0 \end{cases} \quad (5)$$

In general, this model simplifies the complex changes in the timber-burning process and quantifies the thermal effect of timber combustion. For example, as shown in Fig. 8b and 8c, when the Q_{fire} reaches 50 kW/m^2 in the heating stage from 0 to 125 kW/m^2 and the cooling stage from 125 kW/m^2 to 0, the Q_{total} are 58 and 95 kW/m^2, respectively. Therefore, their corresponding timber combustion heat release $Q_{combustion}$ are 8 and 45 kW/m^2, respectively.

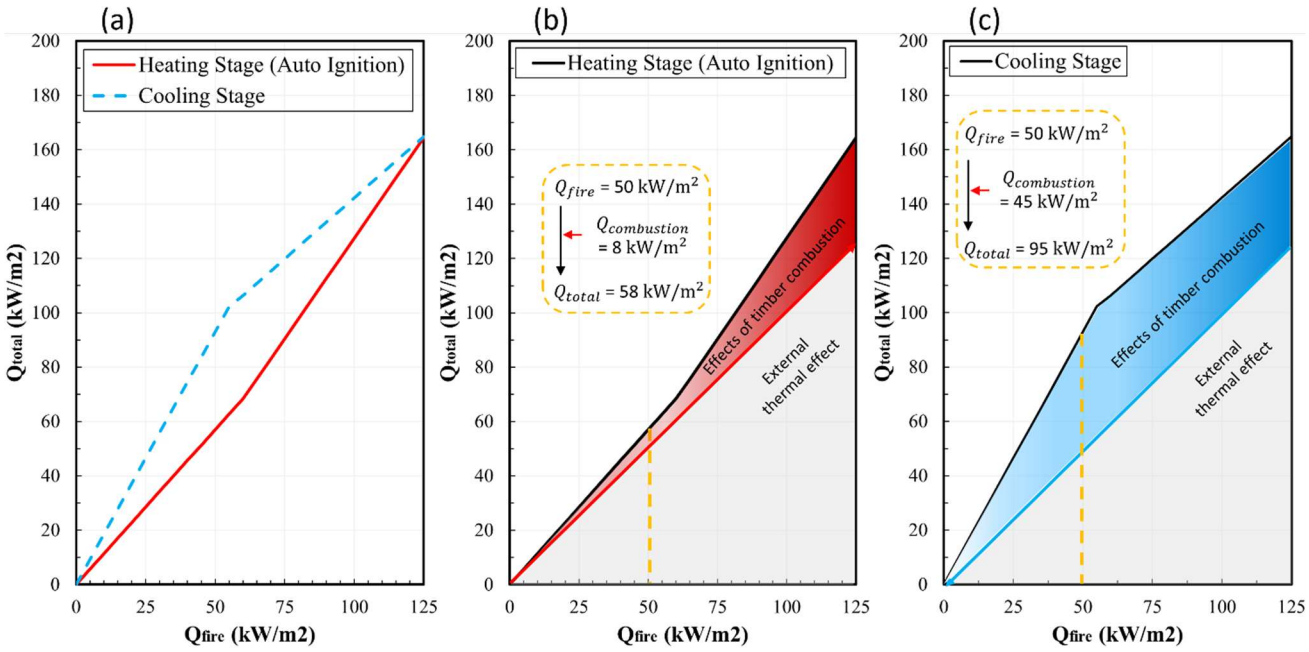

Fig. 8. Proposed heat generation model: (a) Relationship between the external incident heat flux (Q_{fire}) and the received total heat flux (Q_{total}) during heating and cooling stages; (b) Diagram during the heating (Auto ignition) stage; (c) Diagram during the cooling stage.

It is noteworthy that during the cooling phase of the test, while the heat flux gauge wrapped in rock wool board detected a rapid decrease in the incident heat flux Q_{fire}, the detection value Q_{total} of the heat flux meter wrapped in timber block remained stable for a period until Q_{fire} dropped to 110 kW/m^2 before decreasing. This may be due to lagging heating sustained by timber burning despite the reduction of the external heat source. This continued temperature rise during the cooling phase may be due to the lagging heat from timber combustion (smouldering char) despite the reduction of the external heat source. Additionally, even after combustion ceases, ongoing heat transfer and moisture redistribution within the timber can contribute to further delayed failure. These combined effects can potentially result in structural damage or even delayed failure of timber components (for instance, delayed failure of a timber column was observed in [8] and delayed smouldering damage of timber ceilings in large-open timber compartments [9]). However, the current EC5 model and EC5 type model only apply to standard fire exposure and cannot predict the thermal response of timber components in real fire scenarios with non-standard fire actions. Therefore, the proposed model considers the effects

of timber burning on internal heat transfer within the cross-section of timber components during the decay phase, thus improving the fire safety performance of timber structures through more accurate thermal response prediction.

In addition, non-linear models are typically more complex, and simplifying non-linear models into linear versions is an important technique in engineering applications, providing tools that are easier to handle and analyze. Therefore, as shown in Equation (6), the linearized simplified version of the proposed heat generation model is achieved through the bilinear model, which is more user-friendly for processing and analysis.

$$Q_{total} = \begin{cases} \begin{cases} 1.14Q_{fire}, & 0 < Q_{fire} \leq 60 \\ 1.48Q_{fire} - 20.59, & 60 < Q_{fire} \leq 125 \end{cases}, \ heating\ stage \\ \begin{cases} 0.90Q_{fire} + 52.31, & 60 < Q_{fire} \leq 125 \\ 1.86Q_{fire}, & 0 < Q_{fire} \leq 60 \end{cases}, \ Decay\ stage \end{cases} \quad (6)$$

5. Model validation

5.1. The Definition of Thermal Properties Input Parameters for the Validation Cases

The thermal properties of timber have large uncertainties, and various models have been adopted in the literatures [5, 16-18, 29]. The most commonly used model for the thermal properties of timber is the EC5 model. König and Walleij [18] (K&W model) then modified the EC5 model [5] to simulate spruce specimens exposed to Standard fire (SF) and Parametric fires (PF). Using a detailed Gpyro model, Richter et al. [29] adopted the values in Miller and Bellan' s generic wood model (M&B model) [17] to define the thermal properties for different states of timber including virgin layer, dehydration layer, pyrolysis layer and char layer, and estimated the density variation according to mass loss. The values of thermal properties at characteristic temperatures have been listed in Table 2. It can be found that the thermal conductivity values are similarly defined at each characteristic temperature.

Table 2. Thermal properties defined in previous literatures and Eurocode [5, 16-18, 29].

	EC5 model [5]			K&W model [18]			M&B model [16, 17, 29]		
Characteristic temperature	**Density ratio**	k_i **(W/m-K)**	c_{pi} **(J/kg-K)**	**Density ratio**	k_i	c_{pi}	**Density ratio**	k_i	c_{pi}
20 °C	1+ω	0.120	1530	1	0.120	1520	1	0.126	2300
125 °C	1	0.133	2120	0.890	0.135	1640	-	-	-
300 °C	0.76	0.097	710	0.720	0.097	1167	0.349	0.084	1100
600 °C	0.26	0.350	1650	0.625	0.350	690	0.013	0.800	880

The above-mentioned models have been illustrated in Fig. 9, where the input parameters (Table 3)

used in the thermal property of the developed OPS model (Table A.1-C_p, A.1-ρ and A.1-k in Appendix) for non-standard fire (NSF) actions are based on the model values provided in the EC5 only after adjustment according to the relationship between the conductivity and the wood density [37] while variations in density and specific heat follow the EC5 model. For the M&B model associated with different layer states, the thermal properties according to temperature have been plotted as stepwise variations. It should be pointed out that the definitions of thermal property models remain identical for parametric fires (Case PF-Spruce) and NSF scenarios (Case NSF-beech), whereas the differences only appear in the input parameters such as density, moisture ratio, and the associated changes of thermal conductivity based on density [37]. Moreover, these thermal property variations have been integrated into the open-source implementation so as to not require repeated or complex input from users.

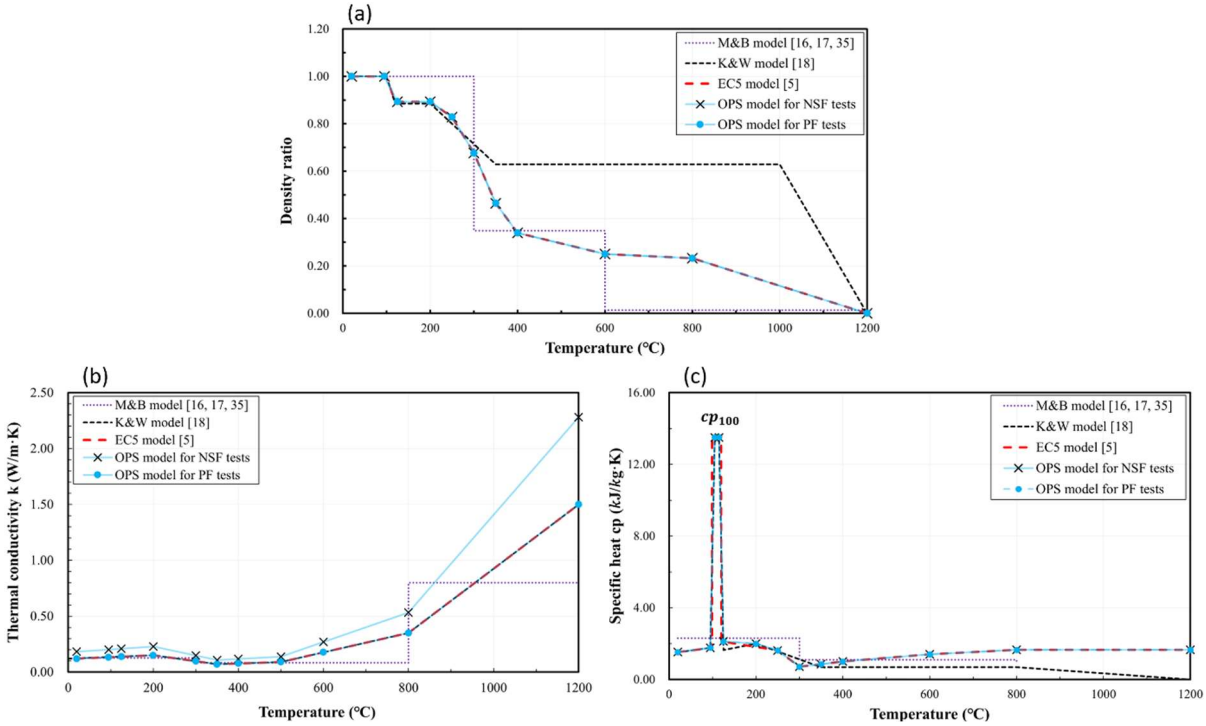

Fig. 9. Thermal properties relationship of timber in literatures and this paper: (a) Density ratio ρ/ρ_{20}; (b) Conductivity k; (c) Specific heat c_p.

Table 3. Input parameters for timber tests in this paper [18].

Variables / Cases	Moisture content (%)	Conductivity k_i (W/m-K)	Density ρ (kg/m^3)	Specific heat c_{pi} (J/kg-K)
	ω	k_{20}	ρ_{20}	c_{p20}
PF-spruce	11.45	0.120	480	1520
NSF-beech [0~125 kW/m^2]	10.88	0.183	730	1520

5.2. Validation against Previous Reference Parametric-fire Tests (König & Walleij [18])

Heat transfer models for the tested specimen are now built in OpenSees for fire, which is capable of 1D, 2D, and 3D heat transfer analyses. A 2D model [34] is used here, and the mesh size along the thickness (depth) is chosen as 1 mm, which can produce nearly identical results compared to the models of finer mesh sizes such as 0.25 mm or 0.5 mm based on sensitivity analysis. For defining the thermal boundaries, the convective heat transfer parameters h is 25 W/m^{2}K on the exposed surface and 1 W/m^{2}K on the unexposed surface. The former is recommended by König and Walleij [18] for modelling in the literature. The transient analysis using central difference and a time step of 0.5s is adopted. Due to a single layer of rock wool board insulating the unexposed surface, only very low convection is applied with h as 1 W/m^{2}K. The emissivity of the exposed timber surface is set as 0.8 [38], whereas no radiation is calculated on the unexposed surface because of insulation. However, the emissivity changes with the phases of the timber surface from virgin wood to burned-out char layer, which were recommended as 0.70 and 0.95 [13, 39].

The PF time-temperature curves imposed as boundary conditions (Fig. 10a and 10b) are the PF-C3 series and PF-C4 series histories reported by König and Walleij [18]. Both curves from tests in a small-scale furnace with internal dimensions 1 m × 0.6 m × 0.6 m (length × width × depth), where the heating profile was defined by the fire load density in MJ/m^2 related to the total area of the enclosure of the fire compartment and the opening factor in m$^{1/2}$. The fire curve for PF-C3 assumes a fire load density of 170 MJ/m^2 and an opening factor of 0.04 m$^{1/2}$, while PF-C4 assumed a fire load density of 510 MJ/m^2 and an opening factor of 0.12 m$^{1/2}$. During the tests, the furnace temperature enters a decay stage after reaching its peak, which was 820 °C in test C1, C2 and C3 (named C3 series) and 1050 °C in test C4, C5 and C6 (named C4 series). Based on the heat generation model with the incident radiant heat flux on the surface of the timber as a reference, the incident radiant heat flux of the furnace gas acting on the surface of the timber is calculated by heat transfer equation and transformed into the total received heat flux taking into account the timber combustion, which is then defined as an external input file and called in the fire model command of OpenSees for fire.

As shown in Fig. 10c and Fig. 10d, with the heat transfer model using the above-described conditions along with the input parameters listed in Table 3, the predicted thermal responses of timber sections remain close to the test data at each depth, which showcases the feasibility study of the present heat transfer model for parametric fires. Among these two cases, relatively larger discrepancies can be observed in the C4 series. The main difference is in the dehydration stage, i.e., the 95~125°C temperature interval, which may be due to the higher actual moisture content of the test samples, while the definition of the specific heat values for this stage in the simulation is based on the moisture content

reported in the literature [18] and EC5 recommended values, which leads to a lag in the temperature rise at each depth. In both cases, the temperature at 6 mm decreases following the decline of furnace temperature. The increment of charring depth slows down after one hour of exposure.

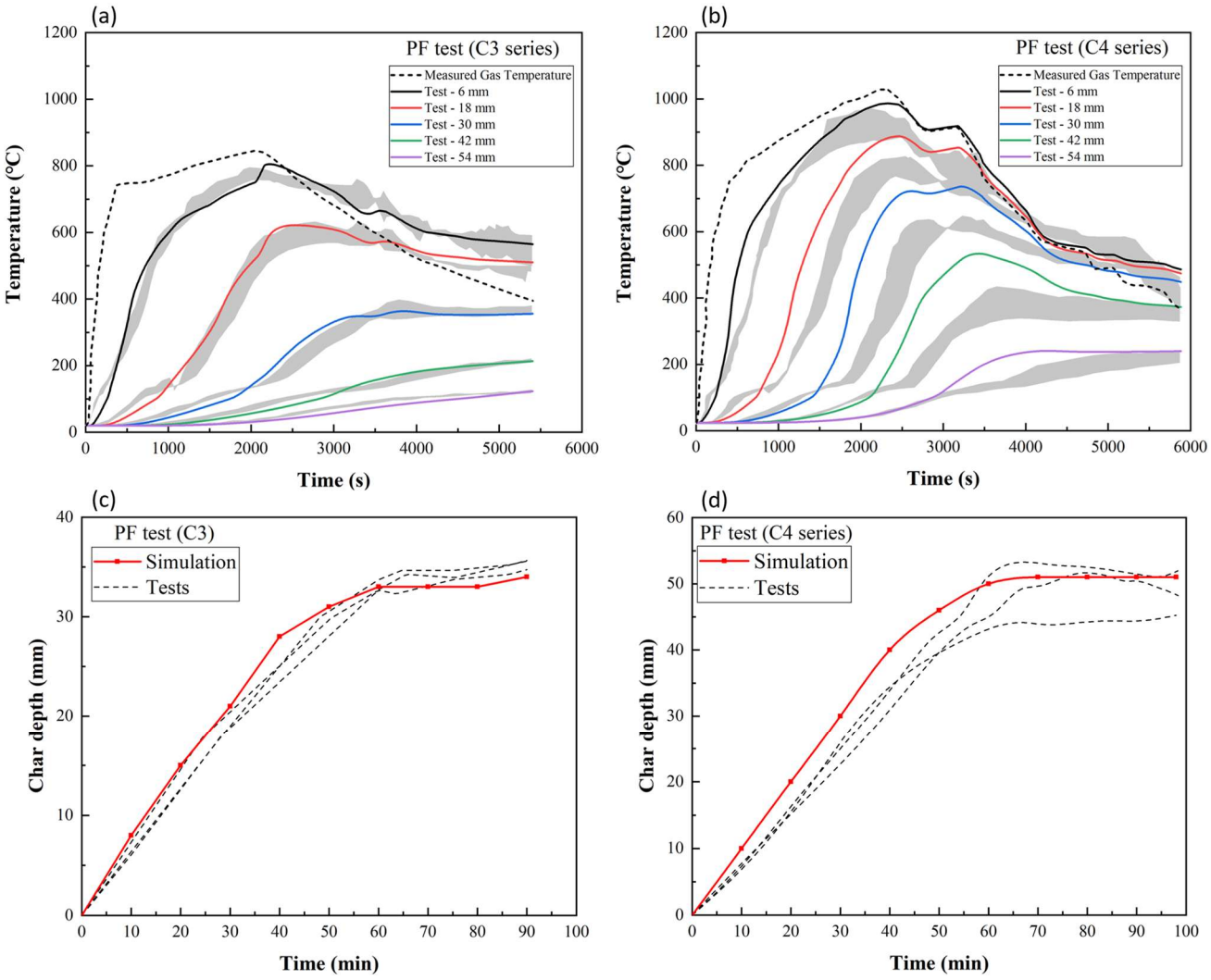

Fig. 10. Thermal response of C3 series and C4 series [18] specimens under the parametric fire: (a) Temperature evolution of C3 series; (b) Temperature evolution of C4 series; (c) Charring depth of C3 series; (d) Charring depth of C4 series.

5.3. Validation against Newly Conducted H-TRIS Time-variant Heat-flux Tests

The non-standard fire (NSF) scenarios are extended to the time-variant heat fluxes as shown in Fig. 11a, which was obtained through varying the power control and panel locations of H-TRIS as described in Subsection 3.2. Based on the proposed heat generation model in Subsection 4.4 and the incident heat flux ($\boldsymbol{Q_{fire}}$) applied to the timber block, the applied heat fluxes ($\boldsymbol{Q_{total}}$) used for heat transfer analysis under non-standard fire actions after considering heat release from timber combustion are shown in Fig. 11b, where the data exceeding the upper limit of the model are extrapolated based on linear fitting. Furthermore, with the heat transfer model using the above-described conditions along

with the input parameters listed in Table 3, the estimated thermal response of the timber section subjected to prescribed non-standard fire (NSF) action of nearly 3200 s are shown in Fig. 11c.

As can be seen from the temperature evolution, the simulated values at 20 mm are a little larger than the tested value between 500 s and 1200 s. This may be because the finite element simulation based only on the defined thermal properties cannot reflect exactly the same physical changes, such as shrinkage and cracking, which causes large errors. In addition, in view of the data fluctuation of the thermocouple during the 800 ~ 1400 s, the failure of the corresponding equipment is also possible. Compared with the test measured data at other thermocouple depths, the heat transfer model has been able to predict well-agreed temperature evolution, except for the removed 30 mm thermocouple with faulty. The above comparison shows that the present model can be used to predict the temperature distribution in the timber cross-section under non-standard fire actions.

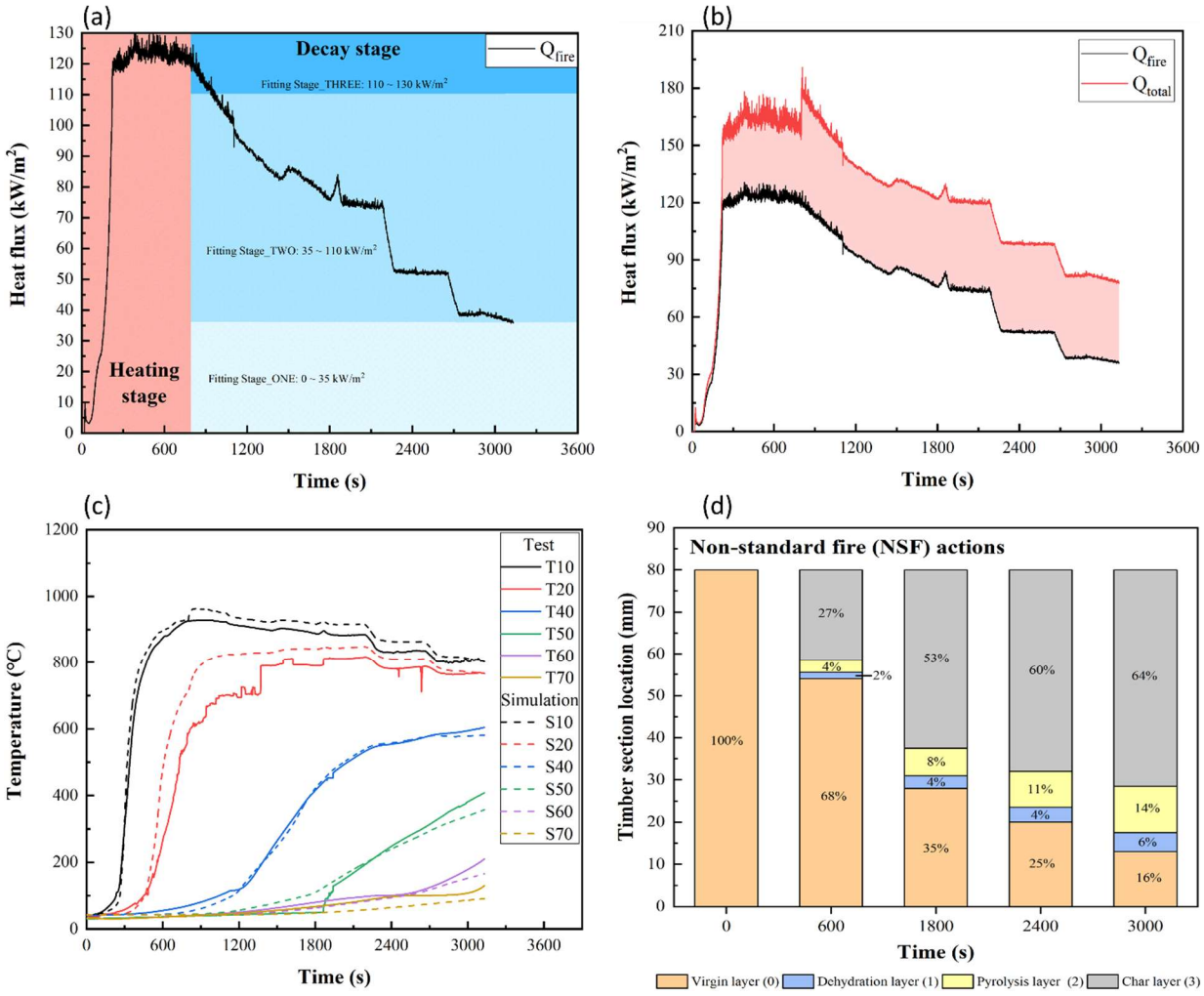

Fig. 11. Timber block exposed to prescribed non-standard fire (NSF) actions: (a) Time-variant incident heat flux (Q_{fire}) subjected to timber block; (b) Applied heat flux (Q_{total}) for simulations based on Q_{fire} and heat generation model; (c) Comparison of measured and simulated temperature-time curves at different depths; (d) Layer distribution of timber block at different time nodes.

Within OpenSees for fire, additional output has been developed for the timber material so that each finite element carries a phase tag, allowing users to track the real-time distribution of virgin wood, dehydration, pyrolysis, and char through the section. Fig. 11d is generated directly from these tags and reports the layer proportions at 0, 600, 1800, 2400 and 3000 s, with coloured columns representing the four states. While the pyrolysis layer is thinner than the char layer at any given time, Fig. 11d shows that during the decay (cooling) stage the growth of char slows, whereas the dehydration and pyrolysis layers continue to expand in relative proportion. This behaviour indicates that, even as external heat flux decreases, thermal inertia in the heated outer region sustains inward heat conduction and the effect of heat generation from timber combustion drives further moisture evaporation and decomposition deeper into the timber. The result is a lag between surface exposure and internal degradation, such that the greatest affected depth may occur after the peak heating stage. From the perspective of materials, dehydration and pyrolysis substantially reduce stiffness and strength before timber converts char, so the zero-strength layer extends beyond the visible char depth. The continued growth of dehydration and pyrolysis during cooling therefore enlarges the ineffective cross-section and can markedly reduce residual capacity, especially in long-decay fires where heat has more time to penetrate. Designs or assessments that consider only the heating phase risk underestimating post-fire damage depth and overestimating residual strength. Accordingly, performance-based evaluations should include the full natural fire curve, including decay, and explicitly check residual section and stability at the end of cooling stage. Overall, the post-peak increase of dehydration and pyrolysis layers captured by the proposed functions of the phase-tag output reflects real physical processes in timber under natural fire.

6. *Discussion on Modelling Thermal Responses of Timber Section in Fire*

The developed heat transfer model for timber sections subjected to non-standard fire actions has been validated using laboratory level tests. It is necessary to clarify that the limitations of the model exist due to the engineering purpose of this model and the scale of test validation. The main purpose of this work is to explore an engineering model for simulating the heat transfer of timber sections subjected to non-standard fire scenarios. The thermal property variation versus temperature has been given based on the literature, and the realistic thermal properties of different timber types may vary. This of course requires more experimental work to achieve a growing database for the broader scope of construction timber. With this model framework, it is possible to develop it further and validate it extensively regarding in-laboratory and full-scale fire tests.

Meanwhile, the realistic fire action to the timber members should be characterized. For fires in modern compartments of more timber components, the fire behavior is significantly affected by the heat released from timber [9-11]. The Malveira large compartment fire test [11] has observed a regional

flashover following the travelling of the fire and the ignition of timber linings at one end of the long compartment. The FRIC-01 test observed rapid flame spread along timber components in an large-open compartment with cross laminated timber (CLT) and large window opening when the ceiling was ignited, but the compartment did not show full flashover but rather a travelling fire behavior with flashing waves [10]. The CodeRed projects have demonstrated the intensified fire behavior induced by the burning of timber ceilings in a large compartment [9]. In the case that a building comprises timber structural members, the ignition of timber will release a large amount of heat to the compartment environment, and the rate of heat release in the compartment will rise rapidly [40]. Thus, the future fire safety evaluation of timber structural members should consider the actual fire impact, which ideally should include the burning of the timber section in the engineering description of fire behavior.

7. Conclusions

This paper presents a heat transfer model aiming to provide an engineering estimation of the thermal response of timber sections in cases where non-standard fire actions are involved. A heat generation sub-model for internally absorbed heat due to combustion has been proposed and integrated into the heat transfer model. The model has been implemented in the OpenSees for fire, taking advantage of the open-source and object-oriented nature of the finite element simulation platform. An investigative case of thermal boundary conditions for timber exposed to non-standard fire actions has been imposed through H-TRIS and conducted to examine the performance of the proposed heat transfer model. The conclusions of this paper are drawn as below:

1) A heat transfer model for timber sections in non-standard fire actions has been developed to incorporate thermal properties, characteristic layer division, and heat generation models.
2) The heat generation models summarized from the tests can be used to effectively assess the amount of heat absorbed within the timber during timber combustion under different fire conditions characterized using different incident radiation heat fluxes imposed by H-TRIS.
3) The proposed heat generation model as an engineering-purposed and simplified model compatible with conventional heat transfer analysis modules has been implemented in OpenSees for fire. Non-standard fire actions including the existing parametric fires tests on the spruces and time-variant heat flux test executed on the beech specimen were used to examine the proposed heat generation model integrated in heat transfer models, and the results showed good performance in predicting the thermal response of timber sections. These test scenarios also demonstrate the need of layer state recording and heat generation model for a heat transfer model of timber sections subjected to non-standard fires.
4) The present work introduces a framework of engineering heat transfer models for timber

sections exposed to fires. Although more experimental studies being needed to enrich the material libraries regarding the timber type and input parameters, the current heat transfer model now provides a modelling basis for further validation and can be potentially used for simulating timber structures in non-standard fire action.

Appendix

Table A.1-c_p. Piecewise specific heat model $c_p(T)$.

Layer Tag (s)	**Temperature range** (°C)	**Evolution expression for Specific heat (c_p) vs Temp (T)** (using c_{p20} as the only input parameter)
Virgin layer (Tag 0)	20 - 95	Linear: $C_p = C_{p20}\ at\ 20\ ℃ \rightarrow 1.16C_{p20}\ at\ 95\ ℃$ (20 - 95 ℃, linear interpolation)
Dehydration layer (Tag 1)	95 - 125	Linear: $C_p = 1.16C_{p20}\ at\ 95\ ℃ \rightarrow 8.82C_{p20}\ at\ 105\ ℃$ (95 - 105 ℃, linear interpolation)
		Constant: $C_p = 8.82C_{p20}\ from\ 105\ ℃\ to\ 115\ ℃$ (105 - 115 ℃, remain constant)
		Linear: $C_p = 8.82C_{p20}\ at\ 115\ ℃ \rightarrow 1.39C_{p20}\ at\ 125\ ℃$ (115 - 125 ℃, linear interpolation)
Pyrolysis layer (Tag 2)	125 - 300	Linear: $C_p = 1.39C_{p20}\ at\ 125\ ℃ \rightarrow 1.31C_{p20}\ at\ 200\ ℃$ (125 - 200 ℃, linear interpolation)
		Linear: $C_p = 1.31C_{p20}\ at\ 200\ ℃ \rightarrow 1.06C_{p20}\ at\ 250\ ℃$ (200 - 250 ℃, linear interpolation)
		Linear: $C_p = 1.06C_{p20}\ at\ 250\ ℃ \rightarrow 0.46C_{p20}\ at\ 300\ ℃$ (250 - 300 ℃, linear interpolation)
Char layer (Tag 3)	300 - 1200	Linear: $C_p = 0.46C_{p20}\ at\ 300\ ℃ \rightarrow 0.56C_{p20}\ at\ 350\ ℃$ (300 - 350 ℃, linear interpolation)
		Linear: $C_p = 0.56C_{p20}\ at\ 350\ ℃ \rightarrow 0.65C_{p20}\ at\ 400\ ℃$ (350 - 400 ℃, linear interpolation)
		Linear: $C_p = 0.65C_{p20}\ at\ 400\ ℃ \rightarrow 0.92C_{p20}\ at\ 600\ ℃$ (400 - 600 ℃, linear interpolation)
		Linear: $C_p = 0.92C_{p20}\ at\ 600\ ℃ \rightarrow 1.08C_{p20}\ at\ 800\ ℃$ (600 - 800 ℃, linear interpolation)
		Constant: $C_p = 1.08C_{p20}\ from\ 800\ ℃\ to\ 1200\ ℃$

		(800 - 1200 ℃, remain constant)

Table A.1-ρ. Piecewise specific heat model $\rho(T)$.

Layer Tag (s)	**Temperature range** (°C)	**Evolution expression for Density (ρ) vs Temp (T)** (using ρ_{20} as the only input parameter) * ω: moisture content, inherent parameter of timber
Virgin layer (Tag 0)	20 - 95	Constant: $\rho = \rho_{20}\ from\ 20\ ℃\ to\ 95\ ℃$ (20 - 95 ℃, remain constant)
Dehydration layer (Tag 1)	95 - 125	Linear: $\rho = \rho_{20}\ at\ 95\ ℃ \rightarrow \frac{\rho_{20}}{1+\omega}\ at\ 125\ ℃$ (95 - 125 ℃, linear interpolation)
Pyrolysis layer (Tag 2)	125 - 300	Constant: $\rho = \frac{\rho_{20}}{1+\omega}\ from\ 125\ ℃\ to\ 200\ ℃$ (125 - 200 ℃, remain constant)
		Linear: $\rho = \frac{\rho_{20}}{1+\omega}\ at\ 200\ ℃ \rightarrow \frac{0.93\rho_{20}}{1+\omega}\ at\ 250\ ℃$ (200 - 250 ℃, linear interpolation)
		Linear: $\rho = \frac{0.93\rho_{20}}{1+\omega}\ at\ 250\ ℃ \rightarrow \frac{0.76\rho_{20}}{1+\omega}\ at\ 300\ ℃$ (250 - 300 ℃, linear interpolation)
Char layer (Tag 3)	300 - 1200	Linear: $\rho = \frac{0.76\rho_{20}}{1+\omega}\ at\ 300\ ℃ \rightarrow \frac{0.52\rho_{20}}{1+\omega}\ at\ 350\ ℃$ (300 - 350 ℃, linear interpolation)
		Linear: $\rho = \frac{0.52\rho_{20}}{1+\omega}\ at\ 350\ ℃ \rightarrow \frac{0.38\rho_{20}}{1+\omega}\ at\ 400\ ℃$ (350 - 400 ℃, linear interpolation)
		Linear: $\rho = \frac{0.38\rho_{20}}{1+\omega}\ at\ 400\ ℃ \rightarrow \frac{0.28\rho_{20}}{1+\omega}\ at\ 600\ ℃$ (400 - 600 ℃, linear interpolation)
		Linear: $\rho = \frac{0.28\rho_{20}}{1+\omega}\ at\ 600\ ℃ \rightarrow \frac{0.26\rho_{20}}{1+\omega}\ at\ 800\ ℃$ (600 - 800 ℃, linear interpolation)
		Linear: $\rho = \frac{0.26\rho_{20}}{1+\omega}\ at\ 800\ ℃ \rightarrow 0\ at\ 1200\ ℃$ (800 - 1200 ℃, linear interpolation)

Table A.1-*k*. Piecewise thermal conductivity model *k(T)*.

Layer Tag (s)	**Temperature range** (°C)	**Evolution expression for Conductivity (*k*) vs Temp (*T*)** (using k_{20} as the only input parameter)
Virgin layer (Tag 0)	20 - 95	Linear: $k = k_{20}\ at\ 20\ ℃ \rightarrow 1.10k_{20}\ at\ 95\ ℃$ (20 - 95 ℃, linear interpolation)
Dehydration layer (Tag 1)	95 - 125	Linear: $k = 1.10k_{20}\ at\ 95\ ℃ \rightarrow 1.15k_{20}\ at\ 125\ ℃$ (95 - 125 ℃, linear interpolation)
Pyrolysis layer (Tag 2)	125 - 300	Linear: $k = 1.15k_{20}\ at\ 125\ ℃ \rightarrow 1.25k_{20}\ at\ 200\ ℃$ (125 - 200 ℃, linear interpolation) Linear: $k = 1.25k_{20}\ at\ 200\ ℃ \rightarrow 0.81k_{20}\ at\ 300\ ℃$ (200 - 300 ℃, linear interpolation)
Char layer (Tag 3)	300 - 1200	Linear: $k = 0.81k_{20}\ at\ 300\ ℃ \rightarrow 0.58k_{20}\ at\ 350\ ℃$ (300 - 350 ℃, linear interpolation) Linear: $k = 0.58k_{20}\ at\ 350\ ℃ \rightarrow 0.75k_{20}\ at\ 500\ ℃$ (350 - 500 ℃, linear interpolation) Linear: $k = 0.75k_{20}\ at\ 500\ ℃ \rightarrow 2.92k_{20}\ at\ 800\ ℃$ (500 - 800 ℃, linear interpolation) Linear: $k = 2.92k_{20}\ at\ 800\ ℃ \rightarrow 12.90k_{20}\ at\ 1200\ ℃$ (800 - 1200 ℃, linear interpolation)

References

[1] Steiger, R. and Fontana, M., "Bending moment and axial force interacting on solid timber beams," *Materials and Structures*. 38(279): p. 507-513. 2005.

[2] Burdurlu, E., Kilic, M., Ilce, A.C., and Uzunkavak, O., "The effects of ply organization and loading direction on bending strength and modulus of elasticity in laminated veneer lumber (LVL) obtained from beech (Fagus orientalis L.) and lombardy poplar (Populus nigra L.)," *Construction and Building Materials*. 21(8): p. 1720-1725. 2007.

[3] He, M., Sun, X., and Li, Z., "Bending and compressive properties of cross-laminated timber (CLT) panels made from Canadian hemlock," *Construction and Building Materials*. 185: p. 175-183. 2018.

[4] Li, Z., He, M., Tao, D., and Li, M., "Experimental buckling performance of scrimber composite columns under axial compression," *Composites Part B: Engineering*. 86: p. 203-213. 2016.

[5] CEN(2004), in EN 1995-1-2. Eurocode 5. Design of timber structures. General. Structural fire design.

[6] Lie, T.T., "A method for assessing the fire resistance of laminated timber beams and columns. ," *Canadian Journal of Civil Engineering*. 4(2): p. 161–169. 1977.

[7] Thi, V.D., Khelifa, M., Oudjene, M., Ganaoui, M.E., and Rogaume, Y., "Finite element analysis of heat transfer through timber elements exposed to fire," *Engineering Structures*. 143: p. 11-21. 2017.

[8] Gernay, T., "Fire resistance and burnout resistance of timber columns," *Fire Safety Journal*. 122. 2021.

[9] Kotsovinos, P., Rackauskaite, E., Christensen, E., Glew, A., O'Loughlin, E., Mitchell, H., Amin, R., Robert, F.,

Heidari, M., Barber, D., Rein, G., and Schulz, J., "Fire dynamics inside a large and open-plan compartment with exposed timber ceiling and columns: CodeRed #01," *Fire and Materials*. 47(4): p. 542-568. 2022.
[10] Bøe, A.S., Friquin, K.L., Brandon, D., Steen-Hansen, A., and Ertesvåg, I.S., "Fire spread in a large compartment with exposed cross-laminated timber and open ventilation conditions: #FRIC-01 – Exposed ceiling," *Fire Safety Journal*. 140. 2023.
[11] Hidalgo, J.P., Goode, T., Gupta, V., Cowlard, A., Abecassis-Empis, C., Maclean, J., Bartlett, A.I., Maluk, C., Montalvá, J.M., Osorio, A.F., and Torero, J.L., "The Malveira fire test: Full-scale demonstration of fire modes in open-plan compartments," *Fire Safety Journal*. 108. 2019.
[12] Morrisset, D., Hadden, R.M., Bartlett, A.I., Law, A., and Emberley, R., "Time dependent contribution of char oxidation and flame heat feedback on the mass loss rate of timber," *Fire Safety Journal*. 120. 2021.
[13] Richter, F. and Rein, G., "A multiscale model of wood pyrolysis in fire to study the roles of chemistry and heat transfer at the mesoscale," *Combustion and Flame*. 216: p. 316-325. 2020.
[14] Richter, F. and Rein, G., "Reduced chemical kinetics for microscale pyrolysis of softwood and hardwood," *Bioresour Technol*. 301: p. 122619. 2020.
[15] Rogaume, T., "Thermal decomposition and pyrolysis of solid fuels: Objectives, challenges and modelling," *Fire Safety Journal*. 106: p. 177-188. 2019.
[16] Huang, X., Rein, G., and Chen, H., "Computational smoldering combustion: Predicting the roles of moisture and inert contents in peat wildfires," *Proceedings of the Combustion Institute*. 35(3): p. 2673-2681. 2015.
[17] Miller, R.S. and Bellan, J., "A Generalized Biomass Pyrolysis Model Based on Superimposed Cellulose, Hemicelluloseand Liqnin Kinetics," *Combustion Science and Technology*. 126(1-6): p. 97-137. 2010.
[18] König, J. and Walleij, L., One-dimensional charring of timber exposed to standard and parametric fires in initially unprotected and postprotection situations, in Rapport / Trätek., ISSN 1102-1071 ; 9908029. p. p. 45. 1999
[19] White, R.H. and Tran, H.C., Charring rate of wood exposed to to a constant heat flux, in Wood Fire Safety: 3rd international scientific conference: The High Tatras, Slovak Republic. p. 175-183. 1996
[20] Wen, L., Han, L., and Zhou, H., "Charring rates of timbers from Chinese species and comparison with various charring rate models," *European Journal of Wood and Wood Products*. 76(4): p. 1347-1351. 2017.
[21] Zhang, Y., Wang, L., and Chen, L., "Energy-based time equivalent approach for evaluating the fire resistance of timber components exposed to realistic design fire curves," *The Structural Design of Tall and Special Buildings*. 30(11). 2021.
[22] Zhang, Y., Zhi, W., Zhang, X., Ni, W., Xu, C., Xu, Y., and Wang, L., "Experimental and numerical study on the validity of the energy-based time equivalent method for evaluating the fire resistance of timber components exposed to travelling fires " *Journal of Building Engineering*. 76: p. 107169. 2023.
[23] Schmid, J. and Frangi, A., "Structural Timber In Compartment Fires – The Timber Charring and Heat Storage Model," *Open Engineering*. 11(1): p. 435-452. 2021.
[24] Lautenberger, C. and Fernandez-Pello, C., "Generalized pyrolysis model for combustible solids," *Fire Safety Journal*. 44(6): p. 819-839. 2009.
[25] Hopkin, D.J., "Predicting the thermal response of timber structures in natural fires using computational 'heat of hydration' principles," *Fire and Materials*. 37(4): p. 311-327. 2013.
[26] Floyd, J. and Hodges, J., "An Approach for Flux and Thickness Scaling of Cone Calorimeter Data for Predicting the Pyrolysis of Materials," *Fire Technology*. 2025.
[27] McKenna, F., Fenves, G., and Filippou, F., (2010) OpenSees, University of California, Berkeley: nd.
[28] Brandt, K., Open spaces in modern materials, in Swedish Wood, Anna Ryberg Ågren. 2019
[29] Richter, F., Kotsovinos, P., Rackauskaite, E., and Rein, G., "Thermal Response of Timber Slabs Exposed to Travelling Fires and Traditional Design Fires," *Fire Technology*. 57(1): p. 393-414. 2020.
[30] Maluk, C. and Bisby, L., A NOVEL TEST METHOD FOR MATERIALS AND STRUCTURES IN FIRE, in The 8th International Conference on Structures in Fire, Tongji University Press: Shanghai. p. 1063-1070. 2014
[31] Maluk, C., Bisby, L., Krajcovic, M., and Torero, J.L., "A Heat-Transfer Rate Inducing System (H-TRIS) Test Method," *Fire Safety Journal*. 105: p. 307-319. 2019.
[32] Manie, J., DIANA User's Manual., 9.4 edn. Delft: TNO. 2010
[33] Jiang, L. and Usmani, A., "Towards scenario fires – modelling structural response to fire using an integrated computational tool," *Advances in Structural Engineering*. 21(13): p. 2056-2067. 2018.
[34] Jiang, L., Jiang, Y., Zhang, Z., and Usmani, A., "Thermal Analysis Infrastructure in OpenSees for Fire and its Smart Application Interface Towards Natural Fire Modelling," *Fire Technology*. 57(6): p. 2955-2980. 2021.
[35] Jiang, L., Chen, C., and Usmani, A., A conceptual timber-steel composite section using char layer as insulation to protect steel, in World Conference on Timber Engineering (WCTE 2021): Santiago, Chile. 2021
[36] Chen, C., Jiang, L., Qiu, J., Orabi, M.A., Chan, W.S., and Usmani, A., "OpenSees development for modelling timber structural members subjected to realistic fire impact," *Fire and Materials*. 47(4): p. 461-478. 2022.
[37] Çavuş, V., Şahin, S., Esteves, B., and Ayata, U., "Determination of thermal conductivity properties in some wood species obtained from Turkey," *BioRes.* 14(3): p. 6709-6715. 2020.
[38] Lucherini, A., Jovanović, B., Van Coile, R., and Merci, B., Background and limitations of the Eurocodeparametric

fire curves, including the fire decay phase, in Proceedings of the 7th International Conference onApplications of Structural Fire Engineering (ASFE'21): Ljubljana, Slovenia. 2021

[39] Huang, X. and Rein, G., "Thermochemical conversion of biomass in smouldering combustion across scales: The roles of heterogeneous kinetics, oxygen and transport phenomena," *Bioresource Technology*. 207: p. 409–421. 2016.

[40] Gorska, C., Hidalgo, J.P., and Torero, J.L., "Fire dynamics in mass timber compartments," *Fire Safety Journal*. 120. 2021.